Removing Intra-1-Hz Covariant Error to Improve Altimetric Profiles of σ^0 and Sea Surface Height

Graham D. Quartly, Walter H. F. Smith, and Marcello Passaro

***Abstract*— Waveform retracking is the process by which a simple mathematical model is fitted to altimeter returns. Over the ocean, the waveform location, the amplitude, and the shape can be fitted by models with 3–5 free parameters, which may, in turn, be linked to geophysical properties of the surface of interest—principally sea surface height (SSH), wave height, and normalized backscatter strength (σ^0, related to wind speed). However, random multiplicative noise, which is due to the summation of power from multiple differently orientated surfaces, produces errors in the estimation of these model parameters. Examination of the correlations among parameters estimated for each waveform leads to simple empirical corrections that reduce the waveform-to-waveform noise in geophysical estimates, resulting in smoother (and more realistic) along-track profiles of σ^0 and SSH. These adjustments are fundamentally dependent upon the waveform model and retracker implemented, but when applied show improved agreement between near-simultaneous measurements from different altimeter missions. The effectiveness of these empirical adjustments is documented fully for MLE-4 retracking of the Jason-3 altimeter, with a reduction in the 1-s variance of σ^0 by 97%. However, the ideas are applicable and beneficial for data from other altimeters, with small improvements in σ^0 for MLE-3 and for AltiKa at Ka-band, while reductions in range variance of ∼40% are noted for most retrackers evaluated.**

***Index Terms*— AltiKa, high-frequency correlations, Jason-3, MLE-3, MLE-4, spectral analysis, waveform retracking.**

I. Introduction

In THE early decades of satellite altimetry over ocean surfaces, the altimetric sea surface height (SSH) error budget was dominated by inadequate knowledge or modeling of spacecraft orbits, ocean tides, radar path delays, and other phenomena extrinsic to the altimeter itself (see [1, Fig. 1]). These errors typically had long (order 100 km and more) correlation lengths along the satellite's path, limiting applications of the data to large-scale studies, unless along-track differences of the radar range data could be exploited without external corrections [2]. More recently, extrinsic errors are no longer the dominant limitation, and as the signal-to-noise frontier has moved to shorter and shorter spatial scales there is increasing interest in mitigating errors arising within the altimeter measurement process itself. This paper is about exploiting intrinsic correlations in altimeter measurement errors to partially mitigate those errors. Here, we expand upon previous studies [3]–[6], extending their work to several altimeters and retrackers, and presenting a method that can be applied generally to any altimeter and retracker.

Manuscript received July 27, 2018; revised December 4, 2018; accepted December 10, 2018. Date of publication January 25, 2019; date of current version May 28, 2019. *(Corresponding author: Graham D. Quartly.)*

G. D. Quartly is with the Plymouth Marine Laboratory, Plymouth PL1 3DH, U.K. (e-mail: gqu@pml.ac.u.k).

W. H. F. Smith is with the National Oceanographic and Atmospheric Administration, College Park, MD 20740 USA.

M. Passaro is with the Deutsches Geodätisches Forschungsinstitut, 80539 München, Germany.

Color versions of one or more of the figures in this paper are available online at http://ieeexplore.ieee.org.

Digital Object Identifier 10.1109/TGRS.2018.2886998

A. Background and Previous Studies

A spaceborne radar altimeter operates by emitting short radio wave pulses and recording their echoes from near-nadir locations on the Earth. Over the open ocean, the pulse may usually be considered to be randomly scattered from a "homogeneously rough" surface, meaning that the probability of echo power is directly proportional to the surface area illuminated by the pulse. In this case, the statistical expectation for the backscattered power as a function of time elapsing within the echo has a simple mathematical formulation [7]–[9]. This will not be the case, if the instrument footprint also contains inhomogeneities, whether due to land, falling rain [10], very calm ("glassy") seas [11], patchy sea-ice, oil slicks [12], or large internal solitary waves [13]. Furthermore, given that the vertical scale of variations due to wind waves and swell in the scattering area (the radar's "footprint") greatly exceeds the radar wavelength (22 mm for Ku-band), the random power fluctuations in each echo [see Fig. 1(a)] will have an exponential distribution, such that the fluctuation variance is equal to the square of the mean power, a phenomenon often called "speckle" in the radar literature.

A conventional altimeter emits pulses at a pulse repetition frequency (PRF) of a few kilohertz, a rate expected to yield a sequence of echoes with little or no echo-to-echo correlation in the random variations in speckle [7], [14]–[18]. It forms the simple ("incoherent") average of the power received in a sequence of typically 50–100 echoes obtained over about 0.05 s, producing a "waveform" [see Fig. 1(a)]. Empirical studies of conventional altimeter waveforms confirm that the random fluctuations in power behave as if each echo had realized independent speckle, except for waveform samples at the beginning of the leading edge, where there may be some correlations in returns [19], although this is not a problem for moderate and large wave heights [15], [18].

By fitting parametric models to altimeter waveforms, a process called "retracking," one may estimate various parameters of geophysical interest. Nearly, all retracking schemes

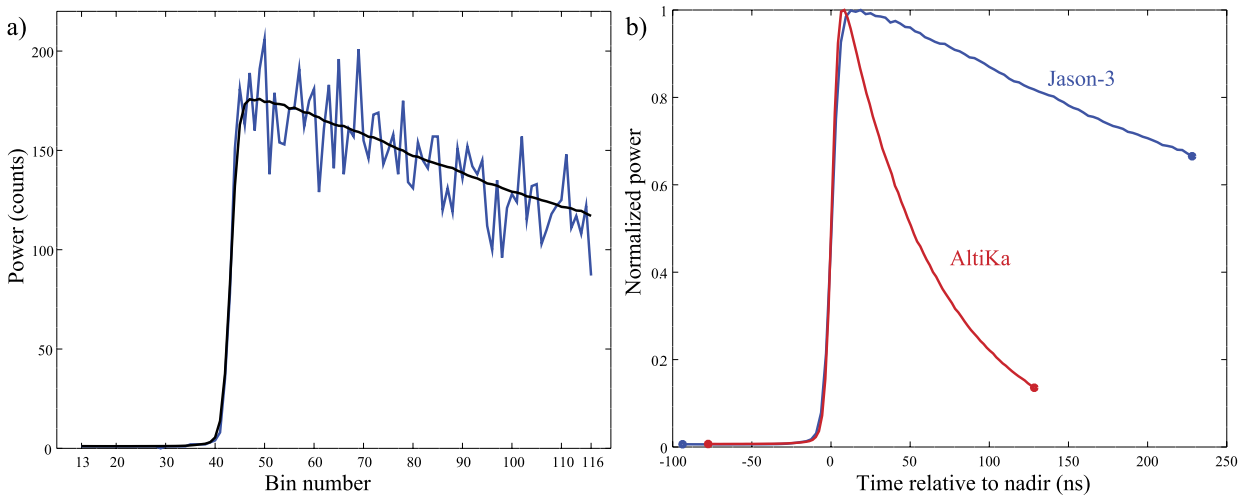

Fig. 1. (a) Illustration of a typical Jason-3 20-Hz waveform (in blue), with a long-period average (in black) indicative of the fitted model. The scatter of observations about the mean waveform is fading noise due to speckle, which is expected to be random and uncorrelated between neighboring bins and between successive waveforms. (b) Comparison of the mean waveform shape for $H_s = 2$ m from Jason-3 and AltiKa. Note both data sets have 104 waveform bins, but the width of the window (in time) is smaller for AltiKa because the sampling rate is every 2 ns, instead of every 3.125 ns as for most Ku-band altimeters. The waveform power rises from background to a maximum and then decays at a rate dependent on the antenna gain pattern. AltiKa, operating in Ka-band, has a decay rate nearly three times that of Jason-3, at Ku-band.

aim to estimate SSH, h, significant wave height, H_s, and normalized backscatter strength, σ^0, from which the wind speed above the ocean may be estimated. Some studies have also estimated the square of an apparent antenna mispointing angle (ψ^2, [20]), the skewness of the surface roughness distribution [9], [21], [22], background instrument noise, or other parameters. Since each waveform is an average of the realizations of a random scattering process, each estimated geophysical parameter is also a random variable.

Previous studies have found that there is an inevitable correlation in the random estimation errors in the parameter estimates of interest. Sandwell and Smith [3] showed that h and H_s must have correlated errors. Quartly [4] examined the correlation between the 20-Hz residuals in σ^0 and ψ^2, and subsequently showed that similar results could be obtained by comparing Jason-1 and Jason-2 20-Hz data during their joint tandem mission [5]. Zaron and deCarvalho [6] did an equivalent analysis for the connection between h and H_s values for Jason-1 and -2 (except that they only used 1-Hz values), producing an adjustment that varied with mean H_s conditions. The concept of exploiting the high-frequency correlations between σ^0 and ψ^2 and between h and H_s was showcased at the Ocean Surface Topography Science Team meeting in 2016 [23]; this paper develops on those ideas with a more robust analysis.

The mathematical model for the waveform expectation is nonlinear in the primary geophysical parameters, and so parameter estimation proceeds by an iterative process that aims to minimize the misfit between the model and the waveform; this process must inevitably take a guided random walk through the model parameter space. Retracking algorithms differ in whether or not they use weighted optimization, whether or not the optimization they use is unconstrained [as is the case for "MLE-3" (3-parameter fit with a so-called "maximum likelihood estimator") [24], "MLE-4" [20], and "PISTACH"] or constrained (as used by Rodriguez and Martin [21], and whether they apply "two-pass retracking" [3], [25], [26]), and what the criteria are for stopping their iterations. Therefore, the correlations among the errors in geophysical parameters are dependent on the retracking algorithm as well as on the nature of the ocean scattering.

Recalling that the instrument footprint has considerable overlap between successive waveforms, we investigate the correlated errors in the high-rate retrievals in order to derive empirical corrections. This paper first repeats the work done by Quartly [4] on σ^0 values from Jason-2 data to show the consistent effect in the latest processing of Jason-2 and Jason-3 data, and then progresses to show how the effect is different for AltiKa. Section IV then extends the work to correct the derivation of range, and again demonstrates that the resultant adjusted values show less noise and more consistency than the standard MLE-4 or MLE-3 products. Section V shows that this empirical adjustment, although simple, needs to be separately defined for each altimeter and each retracker applied to it. Section VI summarizes the work and discusses the applications.

II. Reprise of σ^0 Adjustment

Most modern altimetric satellites have good attitude control such that the boresight of the instrument is pointing directly down to the nadir point, and thus the irradiation pattern is centered on the location giving the earliest returns. In such a case, the expected waveform shape is very well described by a model using the three parameters (h, H_s, and σ^0). However, Jason-1 developed problems with its attitude control, such that it "mispointed" by a significant fraction of the antenna beamwidth. This led to changes in the slope of the waveform trailing edge, which were proportional to the square of that mispointing (hereafter ψ^2).

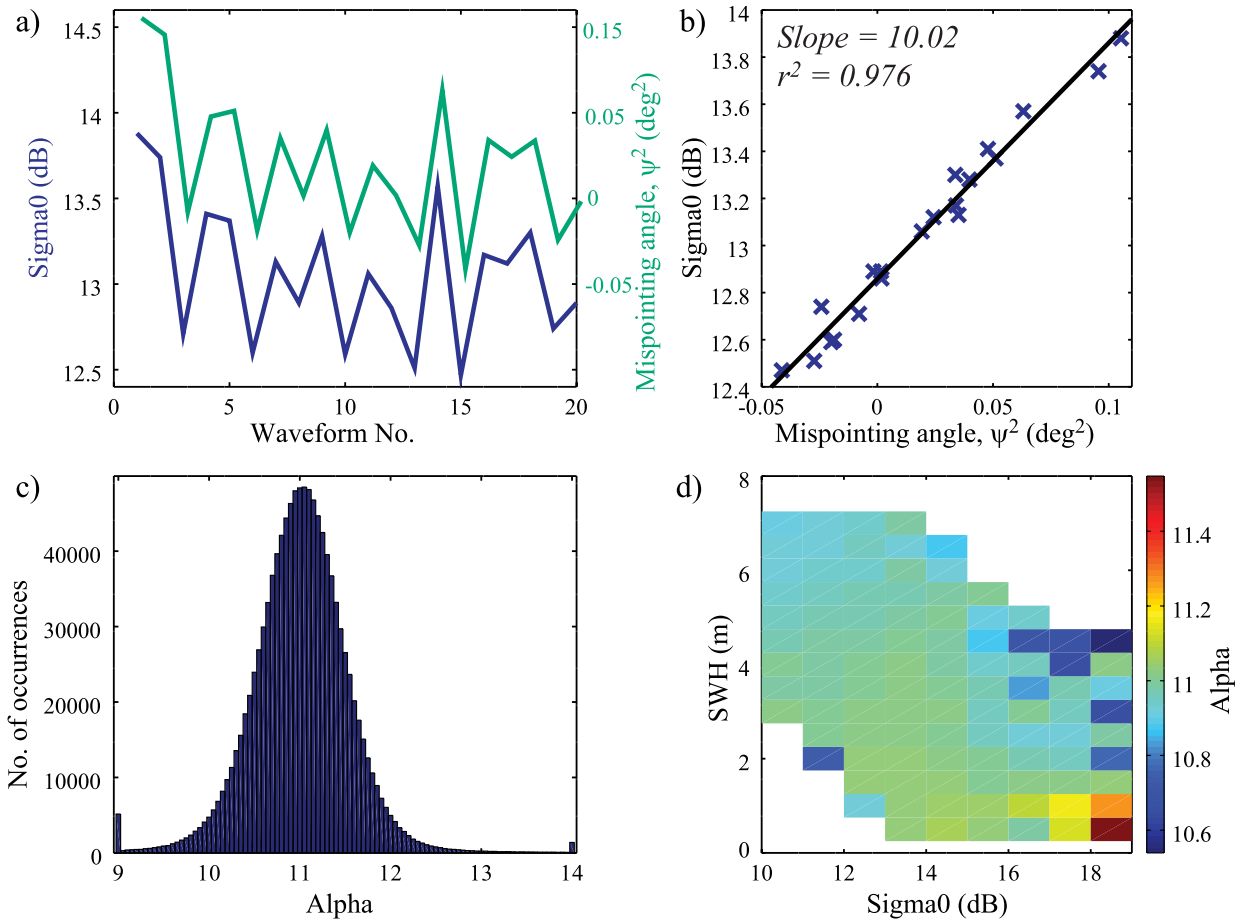

Fig. 2. Correlation of σ^0_{Ku} and ψ^2. (a) Example of 20 observations within a 1-Hz record. (b) Scatter plot of those values with regression slope $\alpha = 10.02$. (c) Histogram of observed values of α for 10 cycles of Jason-3. (d) Variation of mean value of α with wind-wave conditions (characterized by H_s and σ^0).

Amarouche *et al.* [20] introduced the MLE-4 algorithm, which also fits ψ^2 as a fourth unknown, and this approach has become standard. However, as noted by Challenor and Srokosz [27] adding this free variable also affects the constraints on the fitting of σ^0. Consequently, independent 20-Hz estimates of ψ^2 and σ^0 show significant along-track variability that is not physically reasonable, since neither is the platform changing its attitude markedly every 0.05 s nor are the backscatter estimates for highly overlapping footprints that different. Quartly [4] showed that the anomalies (i.e., deviations from the mean) noted for ψ^2 and σ^0 were highly correlated, and later demonstrated that applying similar corrections to both Jason-1 and Jason-2 improved the consistency of their σ^0 values by a factor of three [5].

A. Analysis of Correlation for MLE-4 Estimates From Jason-3

In Fig. 2, we demonstrate that this is still the case for Jason-3, with the latest processing, with the example time series [Fig. 2(a)] showing a high correlation [regression slope, $\alpha = 10.02$, $r^2 = 0.9756$, Fig. 2(b)]. From analyzing 10 cycles of Jason-3 data (i.e., over 1 million 1-Hz records in 99 days), we note that the slope has a median value, α of 11.02 [Fig. 2(c)] with a weak dependence on H_s at very low winds [high σ^0, see Fig. 2(d)]. The spread of values of α [as shown in Fig. 2(c)] is broadly the same for all extant combinations of σ^0 and H_s. This analysis has been repeated for data from the latest version of the Jason-2 Geophysical Data Record (GDR, version E) with essentially the same results. Analysis of a specimen cycle of Jason-2 data from each of its 9 years of mission to-date shows no discernible differences with instrument aging; this is not surprising, as the correlation is principally a result of the chosen retracking approach (as will be shown later).

B. Comparison With MLE-3

Quartly [4] proposed that a more useful estimate of Jason-2's σ^0 values could be achieved by correcting for this observed correlation

$$\sigma^0_{\mathrm{adj}} = \sigma^0_{\mathrm{MLE4}} - \alpha\psi^2 \tag{1}$$

with the expectation that σ^0_{adj} (the "adjusted value") would be like the estimates from MLE-3 (i.e., fitting with ψ^2 constrained to a fixed value), as the output of that reduced model was not then available. As both MLE-4 and MLE-3 estimates are available on the current Jason-3 data stream, it is easy to compare them. Regressing 20-Hz values of $\sigma^0_{\mathrm{MLE4}} - \sigma^0_{\mathrm{MLE3}}$ against ψ^2, we find a very high correlation for the values

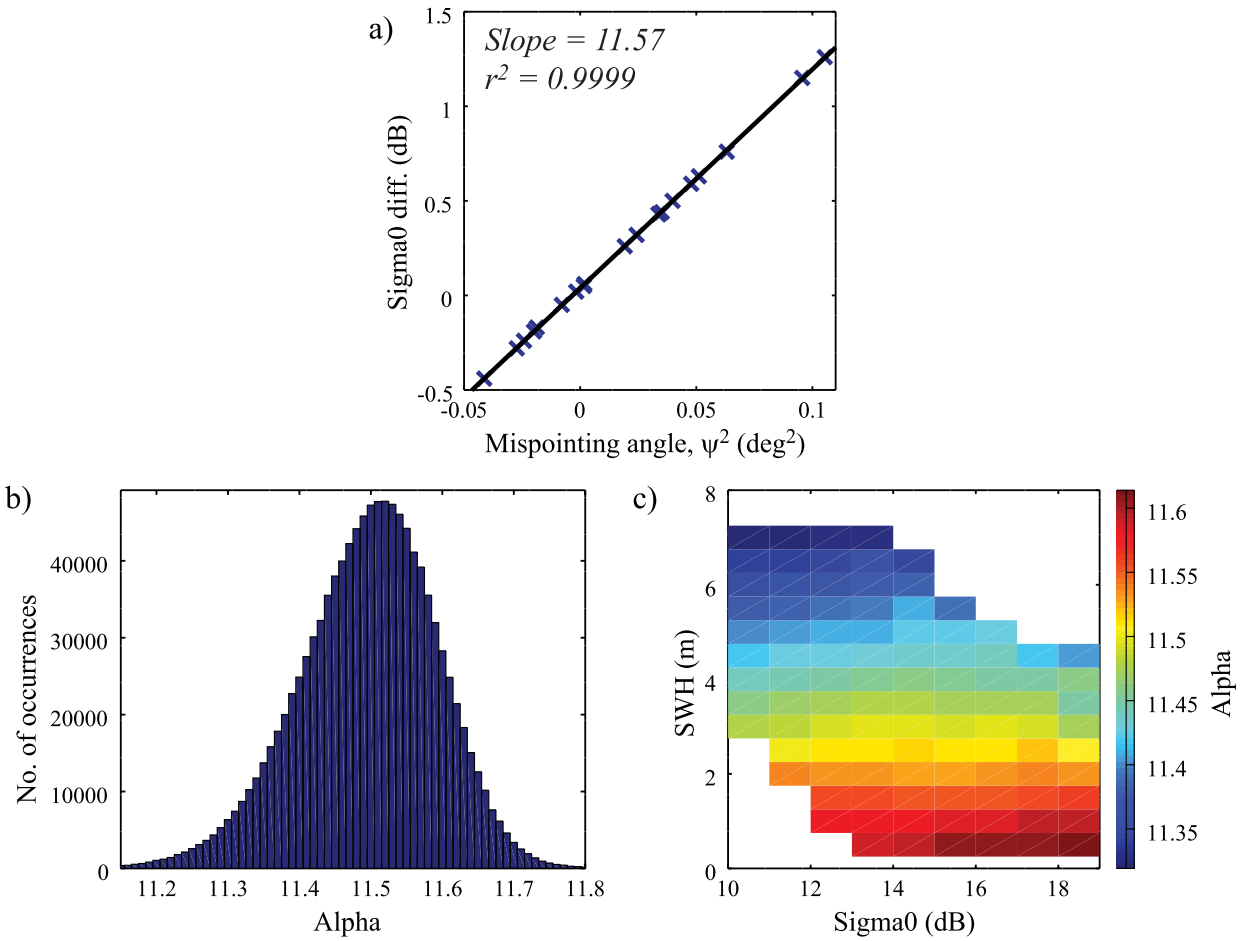

Fig. 3. Correlation of $\sigma^0_{\mathrm{MLE4}} - \sigma^0_{\mathrm{MLE3}}$ and ψ^2. (a) Example scatter plot of 20 observations within a 1-Hz record, with slope α_{4-3} 11.57. (b) Histogram of observed values for 10 cycles of Jason-3 [note that different x-axis scale from that in Fig. 2(c)]. (c) Variation of mean value of α_{4-3} with wind-wave conditions (characterized by H_s and σ^0).

within an individual 1-Hz ensemble [$r^2 = 0.9999$, for the example shown in Fig. 3(a)] and that the regression slope calculated from these many independent ensembles has a mean value of 11.50, with a very narrow range of values (S.D. = 0.10).

The slightly asymmetric histogram of observed slopes [Fig. 3(b)] is due to a variation in the mean value with wave height [Fig. 3(c)] combined with an intrinsic variability (S.D.) of about 0.08 for a given set of conditions. Thus, although the MLE-4 and MLE-3 estimates of σ^0 come from separate retracking algorithms, the output from the MLE-3 retracker can be reliably predicted from the MLE-4 one, as the difference between the two is almost fully specified by the adjustment $\alpha_{4-3}\psi^2$ (where $\alpha_{4-3} = 11.50$), which explains 99.97% of the variance of their difference. The value for α corresponding to the change from σ^0_{MLE4} to σ^0_{MLE3} is slightly greater than that to neutralize the dependence on ψ^2. Thus, in some sense, σ^0_{MLE3} appears slightly overcorrected for the effects of ψ^2.

Quartly [4] had also derived a correction factor for the C-band estimate, σ^0_C, which was, at that time, based on an MLE-3 solution using the value of ψ^2 determined from the MLE-4 applied to Ku-band. In the current version of Jason-2 and Jason-3 data, it is based on an MLE-3 retracker with no input from the Ku-band estimates, and the derived values for α_C are close to zero (mean = −0.02, S.D. = 1.08), and thus we recommend no correction to these values.

C. Reduction in Variability of σ^0

Given that the aim of this empirical adjustment is to reduce the very small-scale variability, it is not surprising that the correction using the simple mean value of α reduces the S.D. within the 1-Hz ensembles; however, the scale of the improvement is impressive (Fig. 4), as the S.D. values noted for MLE-4 are typically reduced by a factor of six. This implies a significant reduction in the standard error of the 1-Hz mean values. The intra-1-Hz consistency achieved by this simple correction is also slightly better than that for the MLE-3 estimations (note that the C-band values also obtained from an MLE-3 estimator are larger than the MLE-3 for Ku-band, because there are far fewer pulses averaged, and thus much more sensitivity to the vagaries of the fading noise).

An interesting demonstration of the improvement in σ^0 values is the much greater consistency between simultaneous estimates at Ku- and C-bands. In many ways, the two different frequencies of Jason-3 can be seen as separate instruments observing the same location simultaneously, although probing at different wavelengths of sea surface roughness. Although, some physical factors affect the two frequencies differently,

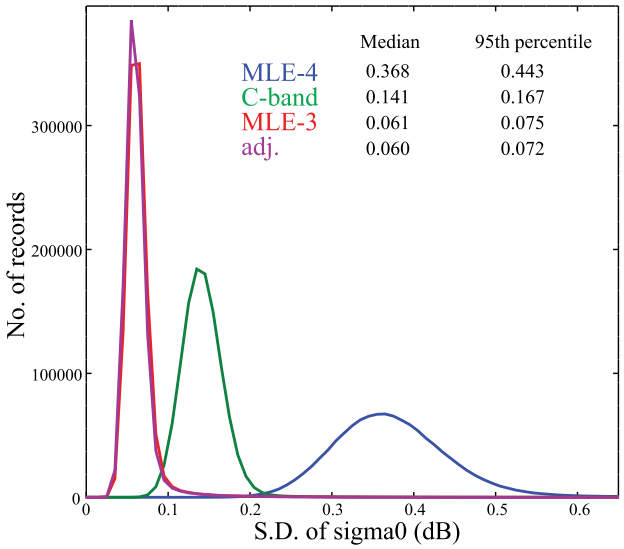

Fig. 4. Histograms of the variability (S.D.) of the 20 σ^0 observations within each 1-Hz record. The magenta curve (labeled "adj") is for the MLE-4 values adjusted according to (1).

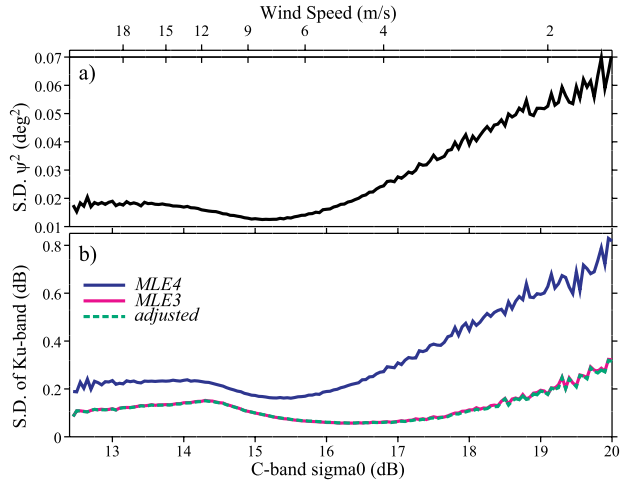

Fig. 5. Variability of ψ^2 causes greater variability of MLE4 estimates of σ^0. (a) Standard deviation of 1-Hz mean values of ψ^2 as a function of σ^0_C (or equivalently, see top axis, of wind speed). (b) Standard deviation of 1-Hz σ^0_{Ku} measurements for given 1-Hz σ^0_C values. The curves for MLE3 and σ^0_{adj} agree to within 2%. [The wind speed axis is derived from the empirical relationship between σ^0_C values and wind speed estimates in the Jason-3 GDRs, as depicted in Fig. 7(a) of [28].]

an improved agreement of the observations at Ku- and C-bands should indicate that the effects of instrument noise have been minimized. The close correspondence between σ^0_{Ku} and σ^0_C is the root of altimetric rain-flagging provided as quality control indicators in the 1-Hz data streams; therefore, we demonstrate the effect of implementing σ^0_{adj} using the 1-Hz values at Ku- and C-bands. As (1) is a linear relation, it is readily applied using the mean of each set of 20 ψ^2 values.

The scatter of the σ^0_{Ku} values from the MLE-4 algorithm for a given σ^0_C value is much greater than the scatter for σ^0_{adj} [Fig. 5(b)], with especially large variations at high σ^0_C values. This is because, in such calm conditions, the spatial scales associated with reflectivity changes are much smaller, so that significant variations within the instrument footprint are likely. This leads to much higher variability in ψ^2 at low

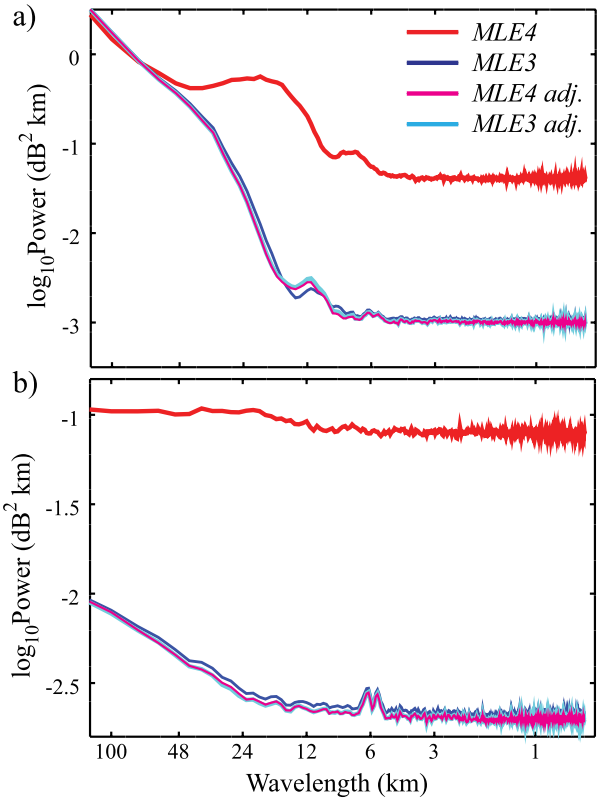

Fig. 6. (a) Spectra of σ^0_{MLE4}, σ^0_{MLE3}, and σ^0_{adj} averaged over many short segments of Jason-3 data with mean H_s close to 2 m. (b) Spectra of difference between Jason-3 and Jason-2 σ^0 values for same conditions.

wind speeds [Fig. 5(a)]. In contrast, the MLE-3 estimates show essentially the same scatter as σ^0_{adj}. An earlier processing of the Jason-2 data did not contain σ^0_{MLE3}, but again σ^0_{adj} showed much greater consistency between the two frequencies than did the MLE-4 estimates [29, Fig. 3(b)]. Since the magnitude of intrinsic scatter affects the threshold on the detection of rain σ^0_{MLE3} and σ^0_{adj} offer almost the same performance, which is much better than using σ^0_{MLE4}. Thus, any useful dual-frequency rain-flagging [30] should be based on one of these robust estimates of σ^0.

D. Spectra of Variations in σ^0

To examine the spatial scales affected by this adjustment, spectra were calculated for sections free from land or ice, using the Welch method with Hamming weighting. Fig. 6(a) shows the mean of 1445 sections for conditions with $H_s = 2$ m, with similar results (not shown) for other wave height regimes. The spectrum for "adjusted" values of MLE-4 (Eq. 1) shows much less variability than its parent retracker at scales smaller than 48 km, and shows very little of the "excess power" feature at 10–48 km.

The reduction in the noise floor at short wavelengths is by a factor of ~50, consistent with the values found for Jason-2 [4]. Note that the spectra for σ^0_{MLE3} and its adjusted version are almost the same as for σ^0_{adj}. This shows that the spectral shape is not particularly sensitive to whether the correction was with a value of α of 11.02 or 11.50, and

indicates that it is not important to model the slight variation of α with environmental conditions [Fig. 2(d)].

A further test of the quality of the correction is afforded by comparisons between Jason-2 and Jason-3 observations during their tandem mission. To avoid interpolation, which effectively applies a smoothing filter to one of the data sets, we compare the satellites using their nearest neighbor points. As Jason-2 provides 20 measurements every 1.020 s, while those of Jason-3 are every 1.019 s, there is a slight mismatch in the spacing, so we constrained the length of observation sections to 1024 points in order that the locations of each would match to within 200 m along track.

There is a little bias between the two instruments (0.25 dB), which has not been removed here; instead, for each of the four flavors of σ^0 being considered, we computed the standard deviation of the 1024 differences and the spectrum of those differences. The mean spectrum for the MLE-4 evaluation is much noisier at all wavelengths considered, while the other three curves are very similar [Fig. 6(b)]. We note an apparent feature at a wavelength of 6 km (and also faintly visible in the spectra of the individual σ_0 profiles [Fig. 6(a)]. This feature was present in $\sim$1% of the difference spectra, but prominent enough to be manifest in the mean; we have not been able to identify its cause.

III. Application to AltiKa

AltiKa is a very different instrument from Jason-3—it is a single-frequency Ka-band altimeter on board the SARAL spacecraft [31]. As the radar frequency is nearly three times that of Jason-3, the operating beamwidth is much smaller, and thus the decay on the trailing edge of the waveform much greater [see Fig. 1(b)]. The width of the emitted pulses is narrower (in terms of travel time), so the slope of the leading edge is slightly steeper for given wave height conditions; the bin-sampling interval is correspondingly finer, so the full recorded waveform is shorter in extent. To allow finer spatial resolution, it records 40 average waveforms per second (as opposed to $\sim$20 for most altimeters), but the speckle characteristics are similar because the higher radar frequency permits a higher rate of independent pulses, and thus a similar number are averaged in each mean waveform. However, the standard processing on the GDRs uses the same MLE-4 code [32], albeit tuned for different instrument parameters. We carried out a similar analysis as for Jason-3 to determine the association between the high-frequency variations in σ^0 and ψ^2 for AltiKa.

For the 40 geophysical estimates within any 1-s ensemble, there is usually a significant correlation between ψ^2 and σ^0, but not with as high r^2 values as shown for Jason-3 [Figs. 2(b) and 3(a)]. The overall distribution of α values for AltiKa does show a broad unimodal distribution, but the breadth of the distribution is greater than the mean or median values [Fig. 7(a)]. The mean is markedly lower than the median due to a long negative tail to the distribution, particularly associated with calm conditions (AltiKa's $\sigma^0 > 13$ dB). A simple overall adjustment of the σ^0 values using (1) with $\alpha = 8.51$ makes a marginal improvement in the consistency

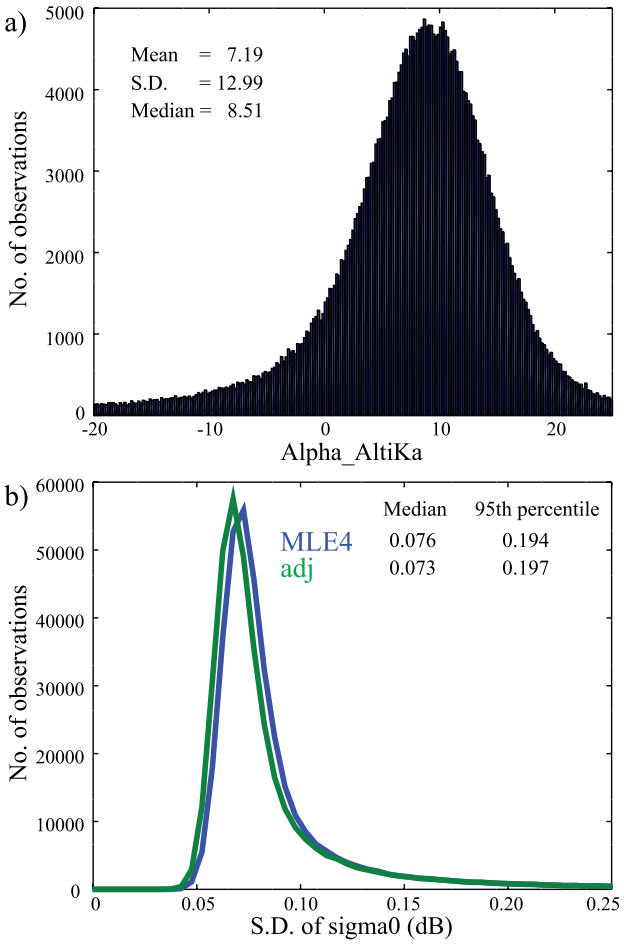

Fig. 7. Determination of σ^0-ψ^2 relationship for AltiKa and its applicability. (a) Histogram of the values of α from 35 days of data (cycle 033). (b) Histograms of the variability of σ^0 within the 40 estimates in each 1-Hz record.

of the 40 values in each 1-Hz record [Fig. 7(b)], but does not reduce the intra-1-Hz variability of those records that were already highly variable.

IV. Extension of Analysis to Correlations of Range and Wave Height

The bins on the leading edge of the waveform contribute significantly to both the estimation of significant wave height, H_s (linked to the slope of the leading edge) and to the epoch (the position of the waveform, which is used to infer the range) [3]. [A host of geophysical and instrumental corrections are added to this latter value to produce the SSH.] A similar intra-1-Hz correlation analysis is carried out to examine the links between these two variables estimated from the leading edge. Rather than use some estimate of SSH that would require selections of geophysical corrections and their interpolation from 1-Hz values, we concentrate on the raw records of altitude minus range, which are fully present at 20 Hz. As there are large-scale along-track changes in altitude minus range due to the varying geoid as well as oceanographic features, the connection between epoch and H_s within a 1-s record is

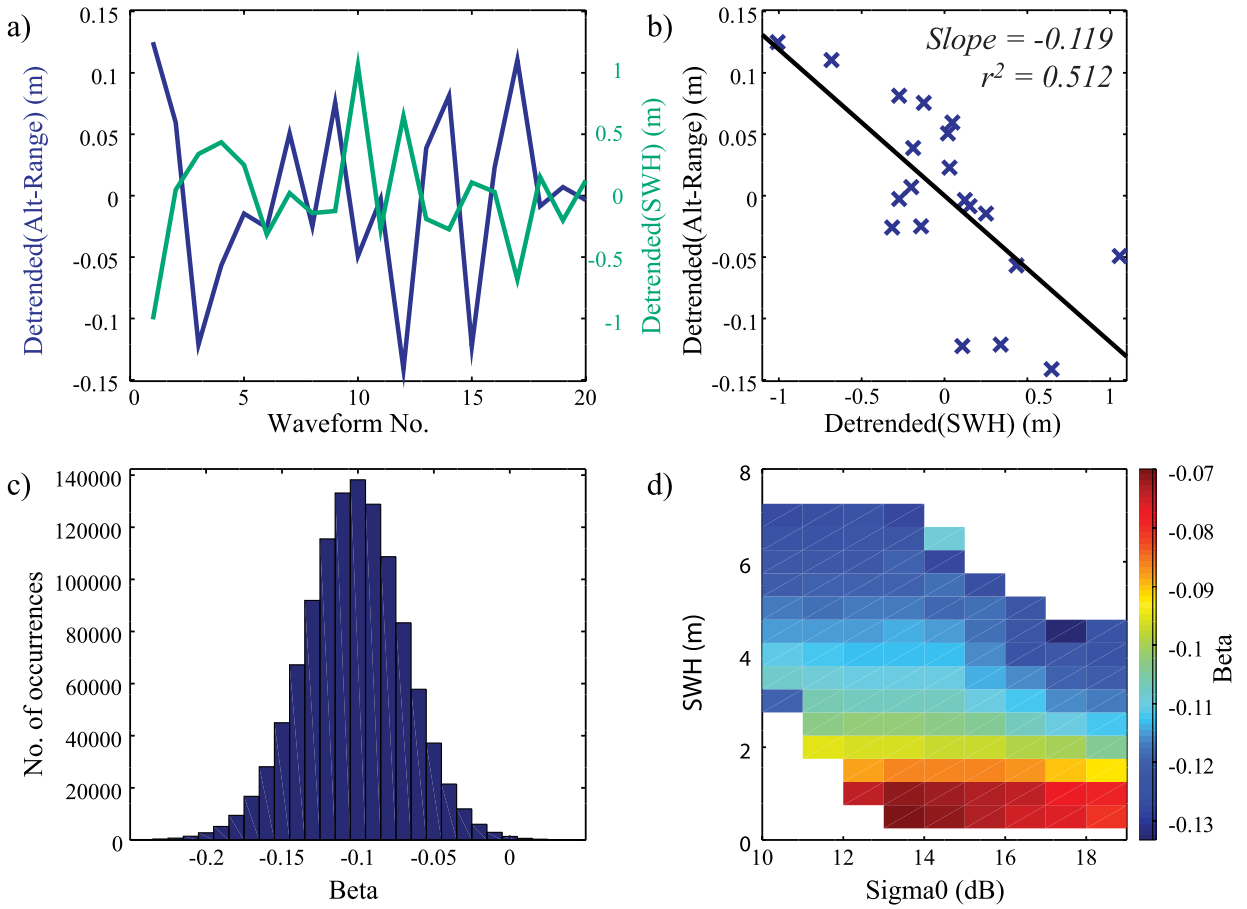

Fig. 8. Correlation of range and significant wave height. (a) Example of 20 observations within a 1-Hz record, with both (altitude minus range) and H_s being detrended to remove larger-scale changes. (b) Scatter plot of those values, with slope $\beta = -0.119$. (c) Histogram of observed values for 10 cycles of Jason-3. (d) Variation of mean value of with wind-wave conditions (characterized by σ^0_{Ku} and H_s).

more easily shown by removing a linear trend from both sets of 20 measurements.

An example set of measurements is illustrated in Fig. 8(a), with a clear anticorrelation between the two series; the display as a scatter plot [Fig. 8(b)] shows a regression slope, β, of -0.119, which is determined by ordinary least squares. However, the scatter is much greater than for the $\sigma_0 - \psi^2$ comparison [Fig. 2(b)], with a correspondingly lower value for r^2. The relationship is nonetheless statistically significant, and there is a high consistency amongst the regression slopes found in analysis of 10 cycles of Jason-3 data [Fig. 8(c)] with a median value for β of -0.102. There is also a clear variation with wave height [Fig. 8(d)], which explains the slight skewness observed in the histogram. Similar analysis for the C-band estimates gives a median value for its regression slope, β_C, of -0.094, and the MLE3 estimates gives a median value for β_{MLE3} of -0.091. In the following, we implement an "adjustment" to altitude minus range of βH_s, and investigate the implications:

$$\zeta_{\mathrm{adj}} = \zeta_{\mathrm{MLE4}} - \beta H_s \tag{2}$$

where ζ = (altitude minus range), and β is a simple constant for each retracker. [Note that as we implement this using absolute values of H_s, rather than anomalies, there is an effect on the large-scale variation of ζ; this should eventually be accompanied by an improved sea state bias (SSB) model.] A common measure of the variability within 1-Hz records is σ_h, which is the standard deviation of ζ once a linear trend has been removed. Applying the adjustment using a simple constant value for β of -0.102 makes a marked improvement for all wave height conditions, with reductions in the variance by 30%–40%. [Although the appropriate value of β does vary with H_s, as shown in Fig. 8(d), the extra improvement for modeling this variation is minuscule in comparison with the gain from the simple implementation.]

Fig. 9(a) shows a comparison of the spectra of ζ; as there has been no removal of the geoid, all the curves converge for large wavelengths. Of the conventional retracking solutions, MLE-4 can be seen to provide a lower noise level than MLE-3, especially in the 6–24-km range associated with the "spectral bump" [33]. However, the proposed adjustment of (2) reduces the noise levels of both these retrackers over all scales less than 24 km, with the noise level at subkilometer scales being 30% less. This improvement is equally clear when applied to the differences between matched observations of Jason-2 and Jason-3 during the tandem phase [Fig. 9(b)]. In this case, the geoid and all geophysical corrections are in common and cancel out.

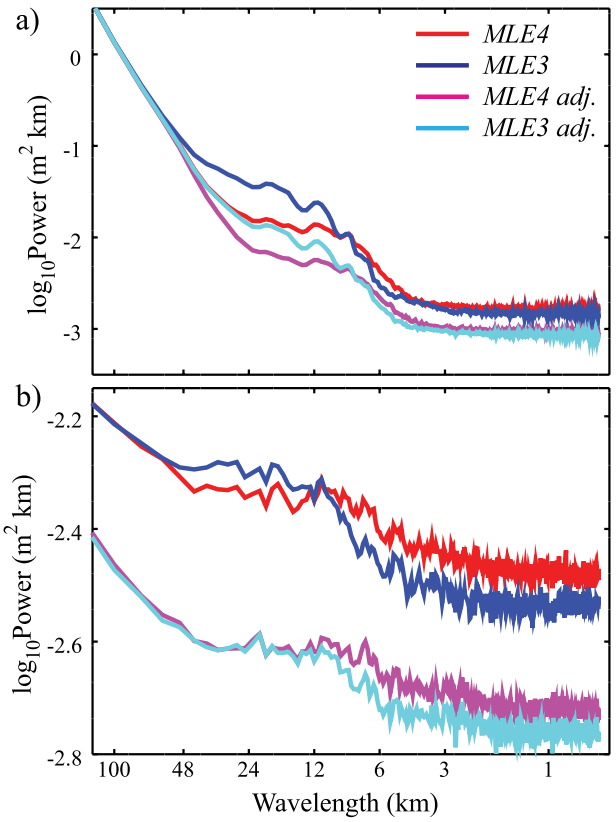

Fig. 9. (a) Spectra of ζ_{MLE4}, ζ_{MLE3}, and ζ_{adj} averaged over many short segments of Jason-3 data with mean H_s close to 2 m. (b) Spectra of difference between Jason-3 and Jason-2 values for same conditions.

V. Application to Other Retrackers

A. Assumptions of Alternative Retrackers

Although the MLE-4 is the standard inversion technique applied on the GDRs of most current altimeters, a number of other retrackers have been developed to offer improved performance in various scenarios. Of particular interest has been adaptive leading-edge subwaveform (ALES) [26], [34], which was designed principally for use in the coastal zone. It reduces the impact of land reflections, which start to manifest themselves in the trailing edge of the waveform, by focusing the inversion only on those waveform bins straddling the leading edge. Consequently, it does not attempt to estimate ψ^2, as the relevant bins for that are in the trailing edge. However, it does use the bins on the leading edge for the determination of both the range and the wave height. The wave height estimates from the ALES retracker have been separately validated [35].

Another variant has been the use of a fully measured shape for the emitted pulse (rather than a Gaussian approximation), which has been implemented within the PEACHI project [36]. This project has implemented two different computational approaches to locating the fitted waveform with the least error: Newton–Raphson (N–R) and Nelder–Mead (N–M). [The N–R is an unweighted fit driving the iteration with gradient-minimizing steps, and so behaves essentially as MLE-4 but with the numerical point target response (PTR), rather than its Gaussian approximation; the N–M is a weighted fit with iterations driven by a downhill simplex crawl; the primary difference in the results of the two methods comes from the weighting of N–M and nonweighting of N–R, rather than from the iteration scheme. The difference between an actual PTR and its Gaussian approximation is irrelevant except at the lowest possible values of H_s.]

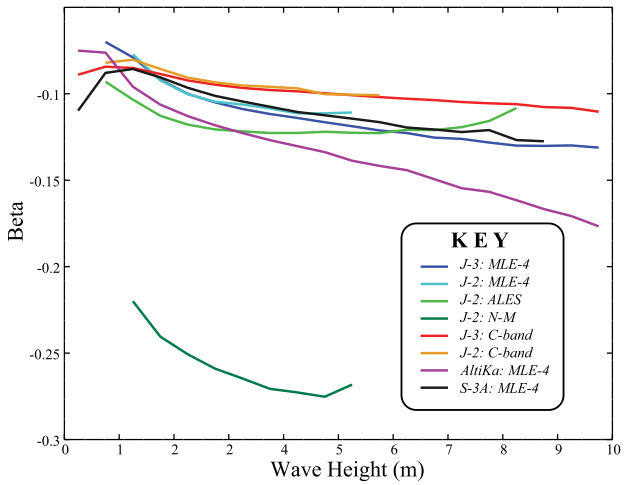

Fig. 10. Variation of β with H_s for various different combinations of altimeters and algorithms.

We have evaluated the association between small-scale anomalies in SSH and wave height for each of these retrackers, and explored how the regression coefficient varies with wave height, since that is the parameter that most governs the shape of the waveform. In Fig. 10, we show the variation in β with H_s for these different retrackers, with a summary of the results for others also included in Table I.

B. Regression Results

The magnitude of the regression coefficient is very much dependent upon the choice of retracker, so there is no simple correction just for each altimeter, but rather for the combination of altimeter and retracker. As would be expected, the α and β values for Jason-2 and Jason-3 are almost the same. Also, for an earlier processing, Quartly [5] showed the mean α_{MLE4} value for Jason-1 to be similar to Jason-2. For σ^0, the S.D. of the adjusted values for Jason-2 and Jason-3 are effectively the same for both MLE-4 and MLE-3 at $\sim$0.060 dB, with the histogram of the values being also close to that for the original MLE-3 estimates (see Fig. 4). Although the median value of α for AltiKa is 8.51, the spread of values is larger, and thus the reduction in variance achieved is only 4%.

For the S.D. of detrended SSH, the empirical adjustment according to (2) reduces the variance for most retrackers by between 35% and 44%, roughly equivalent to the factor of 1.5 to 1.6 noted by Garcia *et al.* [25] for their two-pass processing. The ALES retracker, which was designed for greater resilience in the coastal zone, has a slightly larger σ_h value than the MLE-4 or MLE-3 retrackers when its original data are evaluated over the open ocean. However, as its inversion only uses bins from the first half of the waveform, its β value (showing the correlation of anomalies in H_s and range) is different, and ultimately the "adjusted ALES" retracking solution gives a median σ_h slightly less than the adjusted

TABLE I

MEDIAN VALUES OF SENSITIVITY COEFFICIENTS α AND β FOR VARIOUS DIFFERENT COMBINATIONS OF ALTIMETERS AND ALGORITHMS, AND THEIR EFFECT ON ESTIMATES OF VARIABILITY WITHIN 1-Hz RECORDS

Altimeter / Algorithm	Median α	% Variance explained	Resultant S.D. of σ^0_{adj}	Median β	% Variance explained	Resultant σ_h of h_{adj}
Jason-3/MLE-4	11.02	97%	0.060	-0.102	38%	0.068
Jason-3/MLE-3	-0.48	6.5%	0.059	-0.091	35%	0.065
Jason-2/MLE-4	11.01	97%	0.060	-0.101	38%	0.067
Jason-2/MLE-3	-0.48	6.5%	0.060	-0.091	35%	0.064
Jason-2/ALES				-0.117	50%	0.061
Jason-2/N-R				-0.102	19%	0.111
Jason-2/N-M				-0.252	28%	0.101
S-3A/PLRM	7.84	90%	0.070	-0.095	40%	0.084
S-3A/SARM				-0.095	13%	0.052
Jason-3/C-band	-0.02	~0	0.141	-0.094	44%	0.137
Jason-2/C-band	-0.02	~0	0.140	-0.092	44%	0.135
AltiKa/MLE-4	8.51	4.2%	0.094	-0.116	43%	0.050

Note the values in columns 4 and 7 represent the S.D. within each 1 Hz ensemble; if one assumes the remaining errors are uncorrelated, the standard error (i.e. the uncertainty in the 1 Hz mean) will be less by a factor of $\sqrt{19}$ (or $\sqrt{39}$ for AltiKa).
Values for MLE-4, MLE-3 have been determined from a global analysis; data for N-M, N-R and ALES were from the regional datasets provided.

forms for MLE-4 and MLE-3. The noise reduction in 1-Hz ensembles for C-band and Ka-band is also within that range.

The concept of adjusting for the observed intra-1-Hz correlations may also be translated to nonmarine surfaces. The GDRs for ENVISAT contain the output of a number of different retrackers implemented over all surfaces although they might have specific regions of intended applicability. One such is "ice-2," which is a modification of the Brown model for use over continental ice surfaces, for which there will be some contribution from volume scattering as well as surface scattering. The front half of the shape model is a Gaussian, with the tail described by a fitted exponential. From the Gaussian part, the range and leading-edge width (LEW) are derived. Over marine surfaces LEW^2 approximates to $(H_s^2 + 1.02)/2.82$ (with both LEW and H_s in meters) since both are just descriptors of the slope.

Regression of the intra-1-Hz anomalies over the deep ocean gives a median value for β of ~0.56; application over polar ice shelves (selected as being poleward of 60° and height over 2000 m) gives a median value of ~0.48. This small change reflects the different typical waveform shape, and thus the error characteristics of the waveform space around the minimum model fit error. Apart from at very low LEW, the effective mean β_{ice2} varies between −0.75 and −0.5 according to LEW [Fig. 11(a)]. An adjustment using simply $\beta_{\text{ice2}} = -0.48$ reduces the variance within the 1-Hz ensembles by 15%–30% [Fig. 11(c)].

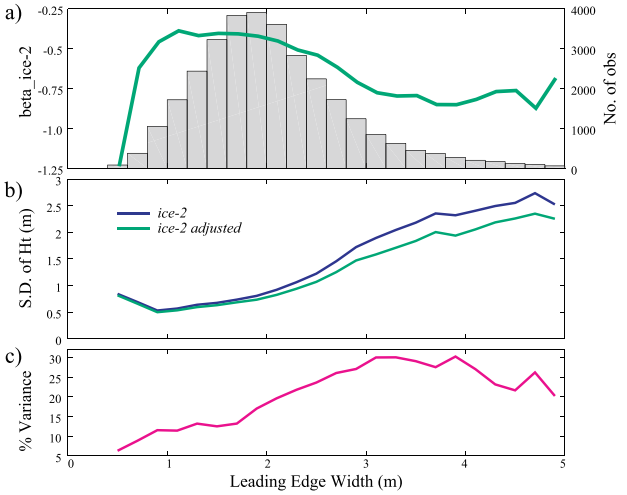

Fig. 11. Example over ice from RA-2 on ENVISAT. (a) Mean value of β_{ice2} as a function of LEW (background plot shows histogram of observations used). (b) Standard deviation of detrended 20-Hz height measurements before and after empirical correction. (c) Percentage reduction in variance.

VI. SUMMARY, DISCUSSION, AND IMPLICATIONS

A. Adjustments to σ^0

In this paper, we have first recapped on the work of [4] and [5] on the intra-1-Hz correlations between MLE-4 estimates of σ^0 and waveform-derived mispointing. Neither property is expected to vary rapidly on such short scales, so their correlation can be used to derive an adjustment that improves the quality of the σ^0 data. This is particularly pertinent for analyses that look at small-scale variability, such as analysis of altimeter data for rain and for oil slicks, or for comparison with point measurements such as meteorological buoys. For climate studies of the large-scale wind patterns or comparison with models (where averages over 50–100 km are used), the adjustment is not usually relevant as the true platform mispointing is normally very small, and thus the waveform-derived values average to near zero over such scales.

Another application of high-frequency σ^0 data has been in the use of wind speed in calculating SSB. This contribution to SSH is normally computed using 1-Hz averages of σ^0 and H_s,

but could be implemented using 20-Hz data [37]. As both the algorithms for converting σ^0 to wind speed and wind speed to SSB are nonlinear, the fluctuations in σ^0 associated with the MLE-4 retracker will produce a small residual error in the SSB correction.

Version E of the Jason GDRs also provided MLE-3 estimates of the parameters, enabling us to show that although derived from a separate retracking process, σ^0_{MLE3} was essentially equivalent to $\sigma^0_{\mathrm{MLE4}} - \alpha_{4-3}.\psi^2$. The extension of the analysis to AltiKa showed that a major change in the waveform shape leads to a different regression coefficient. The investigation of AltiKa waveforms also revealed that as the waveform bins sampled a greater part of the decay in the trailing edge, the perceived effects of changes in backscatter strength and mispointing became more separable. The correlation coefficients for individual 1-Hz samples were then much smaller (not shown), and a wider range of regression coefficients encountered [Fig. 7(a)]. Consequently, the benefits of applying an empirical adjustment are much less [see Fig. 7(b) and Table I].

B. Adjustments to ζ

For decades, there has been concern about errors in altimeter range connected to wave height, with the term "SSB" being the combined effect of three terms. These are skewness (the real physical distribution of the sea surface, with typically sharper wave crests than troughs), electromagnetic bias (different reflecting properties of facets of the sea surface at crests from those at troughs), and retracker bias (an effect inherent to the retracker applied). The work covered in this paper addresses the third term.

Considering first the MLE-4 retracker for Jason-3, we note that while the r^2 value linking ζ and H_s for a typical 1-s ensemble [Fig. 8(b)] is not as large as that linking σ^0 and ψ^2, it is not only statistically significant but also there is a strong consistency between the regression slopes determined for all valid ensembles [Fig. 8(c)]. Although there is a clear but small dependence on H_s, for simplicity, we implement the "adjustment" to SSH as a simple linear function (2). This is sufficient to make a clear reduction in σ_h (the S.D. of the 1-Hz ensemble), and thus in the standard error of the altimetric range. This is further manifested by a reduction in the SSH spectra at scales below 48 km [Fig. 9(a)], and especially in the difference between Jason-2 and Jason-3 in the tandem phase. Section V demonstrates that different values for β are required for different combinations of altimeter and retracker, bringing together for the first time analysis of Jason altimeters, ENVISAT, AltiKa, and Sentinel-3, along with a discussion of different retracking strategies, including the focus of ALES on waveform bins near the leading edge.

These correlated errors have been noted previously by other researchers and estimated or mitigated in different ways. Sandwell and Smith [3] were the first to demonstrate the correlation between estimation errors in ζ and H_s, and particularly how the regression coefficient was markedly different if the retracking used a weighting scheme rather than uniform weighting. Their solution was to run the retracking process over the extent of waveform data of interest, calculate a running mean H_s (over a scale length of order 50 km), and then retrack all waveforms again with all fitted waveforms constrained to have H_s matching the appropriate smoothed value. Garcia *et al.* [25] demonstrated that this methodology removed the "spectral bump." The process suggested in this paper avoids the need for a "two-pass" approach, but achieves similar reductions in noise levels and loss of that bump (see Fig. 9).

Another landmark paper is that by Zaron and deCaravalho [6] who tackled the issue starting from a comparison of the 1-Hz near-simultaneous measurements of Jason-1 and Jason-2, but also investigated the implications for repeat-track analysis, and the change in SSH spectra at short wavelengths. Their results also showed a smaller regression coefficient at low H_s (compare our Fig. 10 and their Fig. 2), although our analysis documents the variation more clearly, since each individual second of data contributes a value for the regression slope, thus permitting more information in the rarer sea state conditions. By starting explicitly at the shortest spatial scales, we have demonstrated an approach that is not dependent upon tandem missions or repeat-track operations, and is readily run on large volumes of data to enable the variation with H_s to be better elucidated. The coastal altimetry community is increasingly interested in finer resolution data from individual waveforms; our adjustments, being derived from such high-rate data, will address their need for corrections evaluated at 20 Hz overall likely values of σ_0 and H_s.

Such ideas have also been pioneered in the cryospheric community, where correlations between LEW and range are used to correct for the effect of different penetration depths [38]–[40]. They use repeat-track analysis, but with full 20-Hz data. Of those published analyses with an LEW-based correction, few show the magnitude of the regression coefficient; however, [39, Fig. 3(b)] shows mainly the values of around -0.8–-0.4 over the Antarctic Plateau. They were interested in a purely empirical correction to compensate for changing local surface conditions, but the values they derived overlap with the range we obtain for our short-scale analysis of the error for the ice-2 retracker.

The magnitudes of the corrections are principally dependent on the retracker applied, rather than the design characteristics of the instrument itself. However, Egido and Smith [18] have shown that for Ku-band altimeters with a PRF of $\sim$2 kHz, there is some correlation of the fluctuations in speckle, especially for bins on the leading edge of the waveform; new retrackers may be envisaged that compensate for this by means of weighted least squares with an error covariance matrix. In such a case, the instrument specification may also have a strong effect on the correlations observed.

The implementation of σ^0_{adj} is fairly straightforward in an operational processing scheme (because there is generally no large-scale variation in ψ^2) and so this was readily incorporated within the RADS processing system (http://rads.tudelft.nl). However, the implementation of ζ^0_{adj} (or an adjusted range) will lead to large-scale changes, because the mean field of wave height varies regionally. Zaron and deCaravalho [6] suggest that the correction be

applied to a high-pass filtered version of H_s, with scales above 100 km removed. An alternative nontrivial solution is to implement the simple form in (2) globally as a correction for short-scale variability due to retracker bias and then rederive an SSB model for the residual terms. Then, this SSB model would have to be applied to a moving-average mean of H_s that represented the genuine scales of variation of H_s, assuming that the skewness and the electromagnetic bias do really vary on those scales. Given that these latter two terms should be instrument-independent for all Ku-band altimeters, one may anticipate that the separation and removal of altimeter-specific retracker bias should enable the unification of SSB models, and allow more effort to be spent on understanding the physical interpretation of the skewness and electromagnetic bias terms.

The benefits of resolving the issues of tracker bias are principally for short-scale studies, where data are not being averaged for 50 km or more along-track or being interpolated to a broad grid. The removal of tracker bias will greatly assist work to derive bathymetry (see [3]), which relies on the differentials of along-track SSH profiles. This empirical adjustment to SSH data should also aid point comparisons with *in situ* tide gages or bottom pressure recorders. It is probably not applicable over rivers and small lakes, as the waveforms there require dedicated processing to account for their different shapes.

ACKNOWLEDGMENT

The authors would like to thank National Oceanic and Atmospheric Administration (NOAA) for the Jason-2 and Jason-3 data, CNES for the AltiKa data, ESA for the ENVISAT data, and Sophie Le Gac for providing some output from the PEACHI processing using Newton–Raphson and Nelder–Mead numerical algorithms. This paper contents are solely the findings and opinions of the authors and do not constitute a statement of policy, decision, or position on behalf of NOAA or the U.S. Government.

REFERENCES

[1] D. B. Chelton, J. C. Ries, B. J. Haines, L.-L. Fu, and P. S. Callahan, *Satellite Altimetry*. New York, NY, USA: Academic, 2001, pp. 1–131.

[2] D. T. Sandwell, "A detailed view of the South Pacific geoid from satellite altimetry," *J. Geophys. Res., Solid Earth*, vol. 89, no. B2, pp. 1089–1104, Feb. 1984. [Online]. Available: https://agupubs.onlinelibrary.wiley.com/doi/abs/10.1029/JB089iB02p01089, doi: 10.1029/JB089iB02p01089.

[3] D. T. Sandwell and W. H. F. Smith, "Retracking ERS-1 altimeter waveforms for optimal gravity field recovery," *Geophys. J. Int.*, vol. 163, no. 1, pp. 79–89, Oct. 2005, doi: 10.1111/j.1365-246X.2005.02724.x.

[4] G. D. Quartly, "Optimizing σ^0 information from the Jason-2 altimeter," *IEEE Geosci. Remote Sens. Lett.*, vol. 6, no. 3, pp. 398–402, Jul. 2009, doi: 10.1109/LGRS.2009.2013973.

[5] G. D. Quartly, "Improving the intercalibration of σ^0 values for the Jason-1 and Jason-2 altimeters," *IEEE Geosci. Remote Sens. Lett.*, vol. 6, no. 3, pp. 538–542, Jul. 2009, doi: 10.1109/LGRS.2009.2020921.

[6] E. D. Zaron and R. DeCarvalho, "Identification and reduction of retracker-related noise in altimeter-derived sea surface height measurements," *J. Atmos. Ocean. Technol.*, vol. 33, no. 1, pp. 201–210, Jan. 2016, doi: 10.1175/JTECH-D-15-0164.1.

[7] T. Berger, "Satellite altimetry using ocean backscatter," *IEEE Trans. Antennas Propag.*, vol. AP-20, no. 3, pp. 295–309, May 1972.

[8] G. S. Brown, "The average impulse response of a rough surface and its applications," *IEEE Trans. Antennas Propag.*, vol. 25, no. 1, pp. 67–74, Jan. 1977.

[9] G. S. Hayne, "Radar altimeter mean return waveforms from near-normal-incidence ocean surface scattering," *IEEE Trans. Antennas Propag.*, vol. AP-28, no. 5, pp. 687–692, Sep. 1980.

[10] T. H. Guymer, G. D. Quartly, and M. A. Srokosz, "The effects of rain on *ERS-1* radar altimeter data," *J. Atmos. Ocean. Technol.*, vol. 12, no. 6, pp. 1229–1247, Dec. 1995, doi: 10.1175/1520-0426(1995)012<1229:TEORON>2.0.CO;2.

[11] J. Gomez-Enri *et al.*, "Modeling Envisat RA-2 waveforms in the coastal zone: Case study of calm water contamination," *IEEE Geosci. Remote Sens. Lett.*, vol. 7, no. 3, pp. 474–478, Jul. 2010, doi: 10.1109/LGRS.2009.2039193.

[12] Y. Cheng, J. Tournadre, X. Li, Q. Xu, and B. Chapron, "Impacts of oil spills on altimeter waveforms and radar backscatter cross section," *J. Geophys. Res., Oceans*, vol. 122, no. 5, pp. 3621–3637, May 2017. [Online]. Available: https://agupubs.onlinelibrary.wiley.com/doi/abs/10.1002/2016JC012568, doi: 10.1002/2016JC012568.

[13] J. M. Magalhaes and J. C. B. da Silva, "Satellite altimetry observations of large-scale internal solitary waves," *IEEE Geosci. Remote Sens. Lett.*, vol. 14, no. 4, pp. 534–538, Apr. 2017, doi: 10.1109/LGRS.2017.2655621.

[14] E. J. Walsh, "Analysis of experimental NRL radar altimeter data," *Radio Sci.*, vol. 9, nos. 8–9, pp. 711–722, Aug./Sep. 1974. [Online]. Available: https://agupubs.onlinelibrary.wiley.com/doi/abs/10.1029/RS009i008p00711

[15] E. J. Walsh, "Pulse-to-pulse correlation in satellite radar altimeters," *Radio Sci.*, vol. 17, no. 4, pp. 786–800, Jul./Aug. 1982. [Online]. Available: https://agupubs.onlinelibrary.wiley.com/doi/abs/10.1029/RS017i004p00786

[16] E. Rodriguez and J. M. Martin, "Correlation properties of ocean altimeter returns," *IEEE Trans. Geosci. Remote Sens.*, vol. 32, no. 3, pp. 553–561, May 1994, doi: 10.1109/36.297974.

[17] M. H. Ka and A. I. Baskakov, "Selection of pulse repetition frequency in high-precision oceanographic radar altimeters," *IEEE Geosci. Remote Sens. Lett.*, vol. 4, no. 3, pp. 345–348, Jul. 2007, doi: 10.1109/LGRS.2007.895679.

[18] A. Egido and W. H. F. Smith, "Pulse-to-pulse correlation effects in high PRF low-resolution mode altimeters," *IEEE Trans. Geosci. Remote Sens.*, to be published, doi: 10.1109/TGRS.2018.2875622.

[19] G. D. Quartly, M. A. Srokosz, and A. C. McMillan, "Analyzing altimeter artifacts: Statistical properties of ocean waveforms," *J. Atmos. Ocean. Technol.*, vol. 18, no. 12, pp. 2074–2091, Dec. 2001, doi: 10.1175/1520-0426(2001)018<2074:AAASPO>2.0.CO;2.

[20] L. Amarouche, P. Thibaut, O. Z. Zanife, J.-P. Dumont, P. Vincent, and N. Steunou, "Improving the Jason-1 ground retracking to better account for attitude effects," *Marine Geodesy*, vol. 27, nos. 1–2, pp. 171–197, Aug. 2004, doi: 10.1080/01490410490465210.

[21] E. Rodriguez and J. M. Martin, "Assessment of the TOPEX altimeter performance using waveform retracking," *J. Geophys. Res., Oceans*, vol. 99, no. C12, pp. 24957–24969, Dec. 1994. [Online]. Available: https://agupubs.onlinelibrary.wiley.com/doi/abs/10.1029/94JC02030, doi: 10.1029/94JC02030.

[22] J. Gómez-Enri, C. P. Gommenginger, M. A. Srokosz, P. G. Challenor, and J. Benveniste, "Measuring global ocean wave skewness by retracking RA-2 Envisat waveforms," *J. Atmos. Ocean. Technol.*, vol. 24, no. 6, pp. 1102–1116, Jun. 2007, doi: 10.1175/JTECH2014.1

[23] G. Quartly, W. Smith, and M. Passaro. (2016). *Intra-1 Hz correlation*. Accessed: Jul. 27 2018. [Online]. Available: https://meetings.aviso.altimetry.fr/fileadmin/user_upload/tx_ausyclss%eminar/files/Intra1Hz_poster_OSTST2016.pdf

[24] O.-Z. Zanifé, P. Vincent, L. Amarouche, J. P. Dumont, P. Thibaut, and S. Labroue, "Comparison of the Ku-band range noise level and the relative sea-state bias of the Jason-1, TOPEX, and Poseidon-1 radar altimeters," *Marine Geodesy*, vol. 26, nos. 3–4, pp. 201–238, Jun. 2003. [Online]. Available: https://www.tandfonline.com/doi/abs/10.1080/714044519, doi: 10.1080/714044519.

[25] E. S. Garcia, D. T. Sandwell, and W. H. F. Smith, "Retracking CryoSat-2, Envisat and Jason-1 radar altimetry waveforms for improved gravity field recovery," *Geophys. J. Int.*, vol. 196, no. 3, pp. 1402–1422, Mar. 2014, doi: 10.1093/gji/ggt469.

[26] M. Passaro, P. Cipollini, S. Vignudelli, G. D. Quartly, and H. M. Snaith, "ALES: A multi-mission adaptive subwaveform retracker for coastal and open ocean altimetry," *Remote Sens. Environ.*, vol. 145, pp. 173–189, Apr. 2014. [Online]. Available: http://www.sciencedirect.com/science/article/pii/S0034425714000534, doi: 10.1016/j.rse.2014.02.008.

[27] P. G. Challenor and M. A. Srokosz, *The Extraction of Geophysical Parameters from Radar Altimeter Returns from a Non-Linear Sea Surface*. Oxford, U.K.: Clarendon, 1989.

[28] G. D. Quartly, "Metocean comparisons of Jason-2 and Altika—A method to develop a new wind speed algorithm," *Marine Geodesy*, vol. 38, pp. 437–448, Dec. 2015, doi: 10.1080/01490419.2014.988834.
[29] G. D. Quartly, "Improving the altimetric rain record from Jason-1 and Jason-2," *J. Geophys. Research: Oceans*, vol. 115, no. C3, Mar. 2010. [Online]. Available: https://agupubs.onlinelibrary.wiley.com/doi/abs/10.1029/2009JC005670, doi: 10.1029/2009JC005670.
[30] G. D. Quartly, T. H. Guymer, and M. A. Srokosz, "The effects of rain on Topex radar altimeter data," *J. Atmos. Ocean. Technol.*, vol. 13, no. 6, pp. 1209–1229, Dec. 1996, doi: 10.1175/1520-0426(1996)013<1209:TEOROT>2.0.CO;2.
[31] N. Steunou, J. D. Desjonquéres, N. Picot, P. Sengenes, J. Noubel, and J. C. Poisson, "AltiKa altimeter: Instrument description and in flight performance," *Marine Geodesy*, vol. 38, pp. 22–42, Jan. 2015, doi: 10.1080/01490419.2014.988835.
[32] P. Vincent *et al.*, "AltiKa: A Ka-band altimetry payload and system for operational altimetry during the GMES period," *Sensors*, vol. 6, no. 3, pp. 208–234, Mar. 2006. [Online]. Available: https://www.ncbi.nlm.nih.gov/pmc/articles/PMC3871951
[33] G. Dibarboure *et al.*, "Investigating short-wavelength correlated errors on low-resolution mode altimetry," *J. Atmos. Ocean Technol.*, vol. 31, no. 6, pp. 1337–1362, 2014, doi: 10.1175/JTECH-D-13-00081.1.
[34] M. Passaro *et al.*, "Cross-calibrating ALES Envisat and CryoSat-2 delay–Doppler: A coastal altimetry study in the Indonesian Seas," *Adv. Space Res.*, vol. 58, no. 3, pp. 289–303, Aug. 2016. [Online]. Available: http://www.sciencedirect.com/science/article/pii/S0273117716301272, doi: 10.1016/j.asr.2016.04.011.
[35] M. Passaro, L. Fenoglio-Marc, and P. Cipollini, "Validation of significant wave height from improved satellite altimetry in the German Bight," *IEEE Trans. Geosci. Remote Sens.*, vol. 53, no. 4, pp. 2146–2156, Apr. 2015, doi: 10.1109/TGRS.2014.2356331.
[36] G. Valladeau *et al.*, "Using SARAL/AltiKa to improve Ka-band altimeter measurements for coastal zones, hydrology and ice: The PEACHI prototype," *Marine Geodesy*, vol. 38, pp. 124–142, Mar. 2015, doi: 10.1080/01490419.2015.1020176.
[37] M. Passaro, Z. A. Nadzir, and G. D. Quartly, "Improving the precision of sea level data from satellite altimetry with high-frequency and regional sea state bias corrections," *Remote Sens. Environ.*, vol. 218, pp. 245–254, Dec. 2018, doi: 10.1016/j.rse.2018.09.007.
[38] B. Legrésy, F. Rémy, and F. Blarel, "Along track repeat altimetry for ice sheets and continental surface studies," in *Proc. Symp. 15th Prog. Radar Altimetry*, Jul. 2006. Accessed: Jan. 9, 2019. [Online]. Available: ftp://ftp.legos.obs-mip.fr/pub/oscar/papers/legresy2006_venice.pdf
[39] F. Rémy, T. Flament, F. Blarel, and J. Benveniste, "Radar altimetry measurements over antarctic ice sheet: A focus on antenna polarization and change in backscatter problems," *Adv. Space Res.*, vol. 50, no. 8, pp. 998–1006, Oct. 2012. [Online]. Available: http://www.sciencedirect.com/science/article/pii/S0273117712002463, doi: 10.1016/j.asr.2012.04.003.
[40] X. Su, C.-K. Shum, C. Kuo, and Y. Yi, "Improved Envisat altimetry ice sheet elevation change data processing algorithms using repeat-track analysis," *IEEE Geosci. Remote Sens. Lett.*, vol. 13, no. 8, pp. 1099–1103, Aug. 2016, doi: 10.1109/LGRS.2016.2567486.

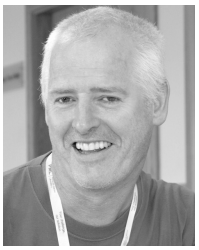

Graham D. Quartly received the B.A. degree in natural sciences from the University of Cambridge, Cambridge, U.K., in 1985, and the Ph.D. degree in underwater acoustics from the University of Bath, Bath, U.K., in 1990.

He was with the U.K.'s Natural Environment Research Council for 23 years, being latterly based at the National Oceanography Centre, Southampton, Southampton, U.K. In 2012, he joined the Plymouth Marine Laboratory, Plymouth, U.K. He was a Principal Investigator or a Co-Investigator of over 10 satellite missions, mostly for altimetry. He is currently a Co-Ordinator of the Expert Support Laboratories for the Sentinel-3 Surface Topography Mission. He is involved in the Climate Change Initiative projects focusing on both sea level and sea state. He has also been heavily involved with in situ work, being a Principal Scientist leading four research cruises. His research interests include the retracking of altimeter data, development of long-term consistent data sets, study of rainfall, and the oceanic circulation within the greater Agulhas system and its wider impacts.

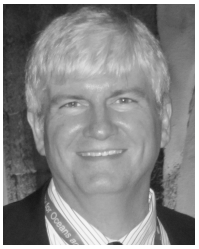

Walter H. F. Smith received the B.S. degree in geological sciences from the University of Southern California, Los Angeles, CA, USA, in 1984, and the Ph.D. degree from Columbia University, New York, NY, USA, in 1990.

From 1990 to 1992, he was a Green Scholar Fellowship with the Scripps Institution of Oceanography, San Diego, CA, USA. Since 1992, he has been a Geophysicst with the Laboratory for Satellite Altimetry, National Oceanic and Atmospheric Administration. He has served on numerous international and interagency committees and science teams. In 2017, he was elected an Honorary Union Fellow with the American Geophysical Union, for his fundamental contributions to marine geodesy, especially applying satellite altimetry to bathymetry, physical oceanography, and oceanic tectonics. He has authored or co-authored more than 60 peer-reviewed papers on topics ranging from the lubrication of plate tectonics to the climatology of the Earth's ionosphere.

Marcello Passaro received the B.S. degree in aerospace engineering from the Politecnico di Milano, Milan, Italy, in 2007, the M.Sc. degree in earth-oriented space science and technology from the Technische Universitaet Muenchen (TUM), Munich, Germany, in 2009, and the Ph.D. degree from the Graduate School of the National Oceanography Centre, Southampton, U.K., in 2016

He is currently a Research Associate with the German Geodetic Research Institute, TUM. His research interests include satellite radar altimetry and its application to sea level and sea state studies.